

Solid Oxide Fuel Cell Modeling

Abraham Gebregergis, *Member, IEEE*, Pragasen Pillay, *Fellow, IEEE*,
Debangsu Bhattacharyya, and Raghunathan Rengaswemy

Abstract—This paper discusses the modeling of a solid oxide fuel cell using both lumped and distributed modeling approaches. In particular, the focus of this paper is on the development of a computationally efficient lumped-parameter model for real-time emulation and control. The performance of this model is compared with a detailed distributed model and experimental results. The fundamental relations that govern a fuel cell operation are utilized in both approaches. However, the partial pressure of the species (fuel, air, and water) in the distributed model is assumed to vary through the length of the fuel cell. The lumped model approach uses the partial pressure of the species at the exit point of the fuel cell. The partial pressure of the species is represented by an equivalent RC circuit in the lumped model.

Index Terms—Fuel cells, modeling, simulation.

I. INTRODUCTION

A SOLID OXIDE fuel cell (SOFC) converts chemical energy into electrical energy at high temperature (800 °C–1000 °C), in contrast to a PEM fuel cell that operates at a lower temperature (80 °C–100 °C). The SOFC is a promising technology for distributed power generation with high efficiency and no moving parts. The transient and static model of an SOFC, which takes into account the effect of electrochemical, thermal, and mass flow, is proposed in [1]. In [2]–[4], dynamic models of SOFCs are developed for analyzing power system performance and fuel cells. A more comprehensive mathematical model of an SOFC is conducted in [5]. It estimates the parameters for a 1-D cathode microstructure SOFC model, such as the composition and particle size. A zero-dimensional model is presented in [6] to show the limitation of the empirical assumptions derived from observation and measurements of physical process. The Butler–Volmer equation analysis for approximating the activation losses in SOFC models is presented in [7]. These papers do not include a detailed analysis of all the losses in a fuel cell. A dynamic fuel cell model, which uses a similar approach to that in [2], is proposed in [8]. Reference [9] focuses only on the effect of polarization losses of an anode-supported SOFC for various cell parameters such as the geometry of the cell. A dynamic model of the SOFC, where a single cell is divided into small control volumes (CVs), is presented in [10]. It is a detailed model that accounts for both

the effects of heat/mass transfer and electrochemical reactions in each CV.

Detailed analyses of interconnecting a fuel cell to a grid are presented in [11]–[15]. References [11]–[14] focus on the design and control algorithms of the power conditioning system only. Reference [15] includes the fuel cell model based on empirical equations derived from experimental data of an actual fuel cell.

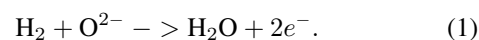
However, the complexity and computation time associated with these models are the drawbacks for real-time emulation and control applications. This paper therefore focuses on a lumped-modeling approach using electrical components in PSpice and/or Matlab/Simulink for real-time applications, and parameter estimation. It also allows the study of the performance and reliability of the SOFC under various flow rates and load conditions. Moreover, the modeling takes into consideration the effects of reactant and product concentrations, polarization losses, and the effects of internal (inherent) resistances. Steady-state simulation results of the SOFC model were compared with experimental data to validate the model.

This paper is organized as follows. Section II is a background study of fuel cell operation, in particular SOFC, followed by two modeling approaches—a distributed model incorporating detailed calculation of all phenomena and a lumped model using electrical components in Section III. The simulation results and experimental data are presented in Section IV. Finally, Section V discusses the conclusions.

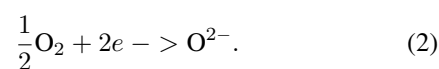
II. SOFC OPERATION

A fuel cell (SOFC) generates electrical power by continuously converting chemical energy of a fuel into electrical energy through an electrochemical reaction. The fuel cell itself has no moving parts, making it quiet and reliable. Fuel cells typically utilize hydrogen as the fuel and oxygen (usually from air) as the oxidant in the electrochemical reaction. It generates electricity, and its by-products are water and heat. The system has higher efficiency compared to conventional combustion engines [16], because it is not limited by Carnot efficiencies. The electrochemical reactions that occur in an SOFC that utilize fuel (hydrogen) and air (oxygen) [1]–[10] are as follows.

Anode:



Cathode:



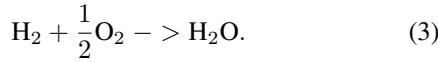
Manuscript received November 9, 2006; revised May 1, 2008. First published November 18, 2008; current version published December 30, 2008. This work was supported by NanoDynamics, Inc.

A. Gebregergis and P. Pillay are with the Department of Electrical and Computer Engineering, Clarkson University, Potsdam, NY 13699-5720 USA (e-mail: natiabraham@gmail.com; pillayp@clarkson.edu).

D. Bhattacharyya and R. Rengaswemy are with the Department of Chemical Engineering, Clarkson University, Potsdam, NY 13699-5707 USA (e-mail: debangsu@clarkson.edu; raghu@clarkson.edu).

Digital Object Identifier 10.1109/TIE.2008.2009516

Overall reaction:



The stoichiometric ratio of hydrogen to oxygen is 2 : 1.

A. Fuel Cell Voltage

The output voltage V_{fc} of the SOFC is given by [1]–[10]

$$V_{fc} = E - V_{act} - V_{con} - V_{ohmic} \quad (4)$$

where E is the Nernst reversible voltage, V_{act} is the activation loss, V_{con} is the concentration loss, and V_{ohmic} is the ohmic loss.

1) *Nernst Reversible Voltage*: The Nernst reversible voltage is the open-circuit voltage of the SO fuel cell when the current density I_{fc} is zero

$$E = E_0 + \frac{RT}{2F} \ln \left(\frac{P_{\text{H}_2} * P_{\text{O}_2}^{0.5}}{P_{\text{H}_2\text{O}}} \right) \quad (5)$$

where $E_0 = 1.1$ V is the standard potential, $R = 8.314$ kJ/kmol · K is the universal gas constant, T is the operating temperature of the fuel cell in kelvins, $F = 96486$ C/mol is the Faraday constant, and P_{H_2} is the hydrogen partial pressure, $P_{\text{H}_2\text{O}}$ is the water partial pressure, and P_{O_2} is the oxygen partial pressure.

2) *Activation Voltage Loss*: Chemical reactions, including electrochemical reactions, must overcome energy barriers, called “activation energy,” for the reaction to proceed. This leads to activation polarization. The activation loss is given by the Butler–Volmer equation [6], [8], [17], [18]

$$I_{fc} = I_0 \left(e^{(\alpha_1 n F / RT) V_{act}} - e^{(-\alpha_2 n F / RT) V_{act}} \right) \quad (6)$$

where I_0 is the exchange current, α_i is the coefficient of charge transfer, and $n = 2$ is the number of moles of electrons transferred.

3) *Concentration Voltage Loss*: This occurs due to the mass transfer resistance to the flow of the reactants and the products through the porous electrodes. Concentration voltage loss can be calculated as [18] and [19]

$$V_{con} = \frac{RT}{nF} \ln \left(\frac{C_b}{C_\infty} \right) \quad (7)$$

where C_b is the concentration at the triple-phase boundary (tpb), where the gas, electrolyte, and electrode meet; C_∞ is the bulk concentration of reactant; and n is the number of moles of electrons participating in the reaction (in this case, $n = 2$).

4) *Ohmic Voltage Loss*: Ohmic losses occur because of the resistance to the flow of ions in the electrolyte and the resistance to the flow of electrons through the electrode materials. The inherent resistance of a fuel cell governed by the change in cell temperature is given by [3], [9], [20], [21]

$$V_{ohmic} = \left(\gamma \exp \left[\beta \left(\frac{1}{T_0} - \frac{1}{T} \right) \right] \right) I_{fc} = r I_{fc} \quad (8)$$

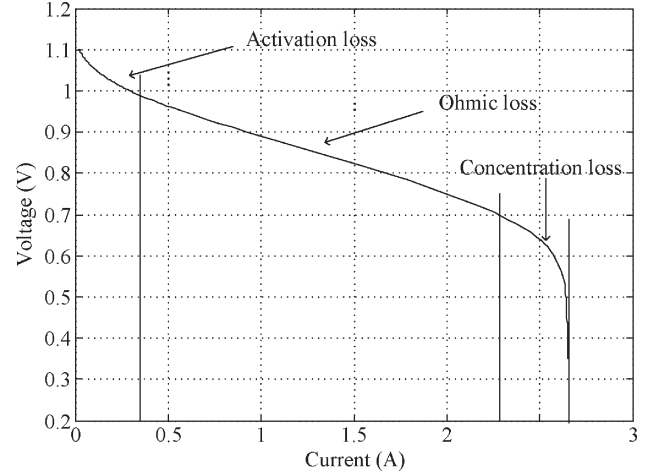


Fig. 1. V – I polarization curve of an SOFC.

where T is the fuel cell temperature; $T_0 = 973$ K, $\gamma = 0.2 \Omega$, and $\beta = -2870$ K are the constant coefficients of the fuel cell; and r is the internal resistance of the SOFC.

Fig. 1 shows a simulated V – I (voltage versus current) polarization curve of a fuel cell. As the cell current begins to increase from zero, a sudden drop of the output voltage of the fuel cell is seen. This drop of the cell voltage is due to activation voltage loss. Then, almost a linear decrease of the cell voltage is seen as the cell current increases beyond certain values, as shown in Fig. 1, which is a result of the ohmic loss. Finally, the cell voltage drops sharply to zero as the load current approaches the maximum current density that can be generated of the fuel cell. The sharp voltage drop is the effect of the concentration loss in the fuel cell.

B. Mass Flow Rate Conservation

The performance of the fuel cell depends on the electrochemical reactions that take place at tpb. A relationship that governs the mass flow rate conservation in the fuel cell is given by [1], [9], [10], [20], [21]

$$\frac{V}{RT} \frac{dP}{dt} = N_x^{\text{in}} - N_x^{\text{o}} - N_x^{\text{r}} \quad (9)$$

where V is the volume of the fuel cell electrode, N^{in} is the input mole flow rate, N^{o} is the output mole flow rate, N^{r} is the mole flow rate reacted, P is the partial pressure, and x is the species.

The electricity generated from the electrochemical reaction inside the fuel cell is given by [8], [9], [16], [20], [21]

$$I_{fc}^r = \frac{4FN_x^r}{n} \quad (10)$$

where n is two for hydrogen and water and is one for oxygen.

III. MODELING THE SOFC

A. Distributed Model

The distributed-modeling approach is introduced here before discussing the lumped SOFC modeling. The cell which

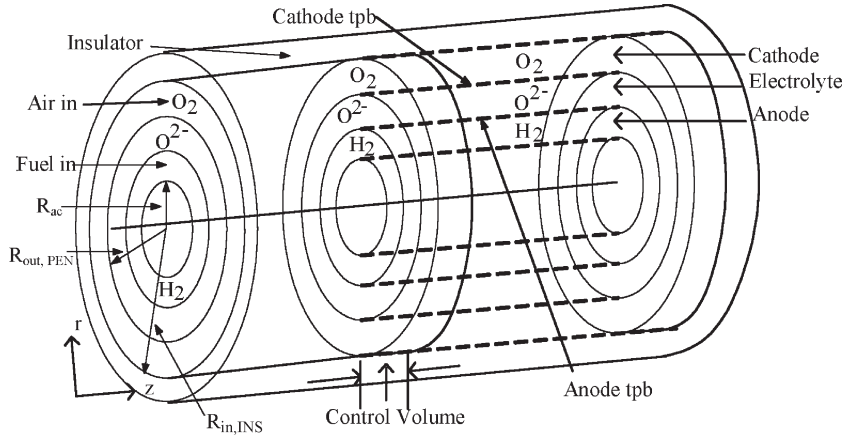


Fig. 2. Schematic of the distributed model of a tubular SOFC.

has been modeled is an anode-supported counterflow tubular SOFC. The modeling considers not only the reactants and product composition but also the physical shape (geometry) of the cell. The modeling is done based on a CV approach, as shown in Fig. 2 [6], [8], [10]. The fuel (hydrogen) enters into the anode channel, and air goes to the cathode channel. The fuel diffuses into the anode tpb through the porous anode, where it reacts with the incoming oxygen ions to produce water. In the same manner, oxygen diffuses into the cathode tpb through the porous cathode. The oxygen ions which are generated in the tpb of the cathode travel through the solid oxide electrolyte to the anode tpb to react with the fuel. The unutilized air and hydrogen are exhausted to the balance of the plant facilities. The fuel and air enters each CV at different concentrations from the cathode channel and the anode channel, respectively. Hence, the partial pressure measured at each CV is different and is a function of time and space. This partial pressure governs the dynamics of the fuel cell.

The species conservation equations in the channels for the distributed SOFC model are as follows [10], [22].

Hydrogen conservation:

$$\frac{\partial C_{H_2}}{\partial t} = -\frac{(\partial C_{H_2} u_{z,ac})}{\partial z} + \frac{2D_{H_2-H_2O_{eff}}}{R_{ac}} \frac{\partial C_{H_2}}{\partial r}. \quad (11)$$

Water conservation:

$$\frac{\partial C_{H_2O}}{\partial t} = -\frac{(\partial C_{H_2O} u_{z,ac})}{\partial z} + \frac{D_{H_2O-H_2O_{eff}}}{R_{ac}} \frac{\partial C_{H_2O}}{\partial r}. \quad (12)$$

Oxygen conservation:

$$\frac{\partial C_{O_2}}{\partial t} = -\frac{(\partial C_{O_2} u_{z,cc})}{\partial z} + \frac{2D_{O_2-N_2_{eff}}}{R_{cc}} \frac{\partial C_{O_2}}{\partial r}. \quad (13)$$

Nitrogen conservation:

$$\frac{\partial C_{N_2}}{\partial t} = -\frac{(\partial C_{N_2} u_{z,cc})}{\partial z} + \frac{2D_{N_2-O_2_{eff}}}{R_{cc}} \frac{\partial C_{N_2}}{\partial r}. \quad (14)$$

$R^2 = R_{in,INS}^2 + R_{out,PEN}^2$, C_x is the molar concentration of species x , u_z is the velocity in the main flow direction z , R_{ac} is the radius of the anode channel, t is the time, D_{x-y}

is the effective binary diffusivity of x into y , $R_{out,PEN}$ is the outside radius of PEN (porous cathode electrode, electrolyte, and porous anode electrode assembly), $R_{in,INS}$ is the inside radius of the insulator, and subscripts ac, an, cc, and ca denote the anode channel, anode, cathode channel, and cathode, respectively.

The momentum conservation equations for the distributed SOFC model are as follows [10], [22].

Anode channel:

$$\frac{\partial(\rho_{ac} u_{z,ac})}{\partial t} = -\frac{\partial(\rho_{ac} u_{z,ac}^2)}{\partial z} - \frac{\partial(\rho_{ac} u_{r,ac} u_{z,ac})}{\partial r} - \frac{\partial p_{cc}}{\partial z}. \quad (15)$$

Cathode channel:

$$\frac{\partial(C_{cc} u_{z,cc})}{\partial t} = -\frac{\partial(\rho_{cc} u_{z,cc}^2)}{\partial z} + \frac{\partial(\rho_{cc} u_{r,cc} u_{z,cc})}{\partial r} + \frac{\partial p_{cc}}{\partial z}. \quad (16)$$

ρ_x is the density in the x channel and p_x is the pressure in the x channel. These equations are developed based on the assumption that u is a function of z and t only. The radial component of the velocity vector is ignored. Since the Reynolds number, the ratio of the rate of the convective transport of momentum to the rate of the molecular transport of momentum, is greater than one in both the anode and cathode channels in the operating range of the cell, the molecular transport of momentum in the main flow direction is ignored.

The species conservation equations in the electrode are as follows [22].

Hydrogen conservation:

$$\epsilon_{an} \frac{\partial(C_{H_2,an})}{\partial t} = \frac{1}{r} \frac{\partial}{\partial r} \left(r D_{H_2-H_2O_{eff}} \frac{\partial C_{H_2,an}}{\partial r} \right). \quad (17)$$

Oxygen conservation:

$$\epsilon_{ca} \frac{\partial(C_{O_2,ca})}{\partial t} = \frac{1}{r} \frac{\partial}{\partial r} \left(r D_{O_2-N_2_{eff}} \frac{\partial C_{O_2,ca}}{\partial r} \right). \quad (18)$$

ϵ_{an} and ϵ_{ca} are the porosities of the anode and cathode, respectively. Similar equations are also written for water and

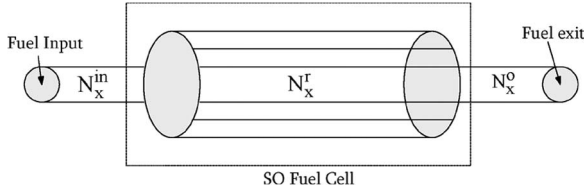


Fig. 3. Tubular SOFC lumped model.

nitrogen conservations. The boundary conditions are listed in Appendix A.

In contrast to the distributed SOFC model, a lumped model that applies the fundamental electrochemical equations and equivalent electrical components is presented next. The model developed is for a single cell. This approach can be easily extended to model “a fuel cell stack.” The proposed model is of reduced complexity and is amenable to real-time applications.

B. Lumped Model

1) *Species Conservation:* In the case of the distributed-modeling approach, the flow rate and partial pressure at each CV are different. The lumped model considers the fuel cell as a single lumped system, which reduces the complexity and computation time. The species enter the cell through one end and leaves through the other end, as shown in Fig. 3. The mass conservation is applied at one end of the fuel cell. The partial pressure at the exit point of the fuel cell is calculated using (9). The relation between the reactant/product flow rate and the cell current of the fuel cells is given by [1]–[10]

$$N_x^r = 2nK_r I_{fc} \quad (19)$$

where $K_r = 1/(8F)$.

The output flow rate N^o of the species at the exit is a function of the current generated by the fuel cell and the inlet flow rate. This output flow rate can be expressed as a function of the partial pressure of the species [2], which is given by

$$N^o = K_x P_x \quad (20)$$

where P_x is the partial pressure of species x at the output and K_x is the molar valve constant of species x .

Substituting (19) and (20) into (9) results in

$$\frac{V}{RT} \frac{dP_x}{dt} = N_x^{\text{in}} - K_x P_x - 2nK_r I_{fc}. \quad (21)$$

Rearranging (21),

$$\frac{V}{RT} \frac{dP_x}{dt} + K_x P_x = N_x^{\text{in}} - 2nK_r I_{fc}. \quad (22)$$

Taking the Laplace transform of (22)

$$\left(\frac{V}{K_x RT} s + 1 \right) P_x(s) = \frac{1}{K_x} (N_x^{\text{in}} - 2nK_r I_{fc}). \quad (23)$$

The boundary conditions of this lumped model are listed in Appendix B.

TABLE I
CHEMICAL-TO-ELECTRICAL EQUIVALENCE

Chemical model	Electrical Model	Description
V/RT	C	Geometry => Capacitor
dP_x/dt	dV/dt	Pressure => Voltage
N_x^{in}	i	flow rate => Current source
$1/K_x$	R	constant => Resistor

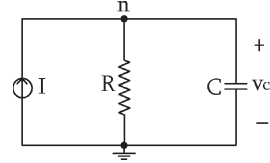


Fig. 4. Electrical model of partial pressure equation.

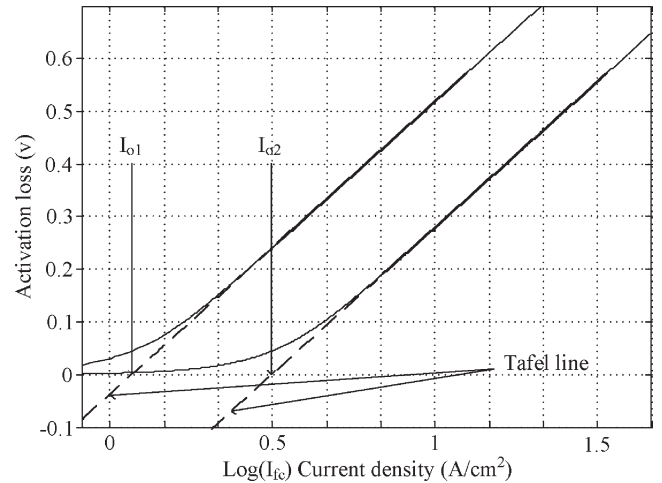


Fig. 5. Activation loss versus logarithmic of current density.

The electrochemical equations given in (23) can be modeled with electrical components using the analogy [23] shown in Table I. Fig. 4 shows an equivalent electrical model representation of the chemical equation that determines the partial pressure of the species. The current at node n in Fig. 4 and its Laplace transform are given in (24) and (25). Since the dynamic response of the fuel cell is contained in the electrochemical equations, the equivalent electrical circuit inherits the dynamics

$$C \frac{dV_c}{dt} = I - \frac{V_c}{R} \quad (24)$$

$$(RCs + 1)V_c(s) = I(s)R. \quad (25)$$

2) *Activation Voltage Loss:* Fig. 5 shows the simulated results of an activation loss versus a logarithm of cell current density of the SOFC. The two dashed straight lines are calculated based on the Tafel equation given in (26) for two different exchange current density I_0 values, i.e., $I_{01} = 1.0689 \text{ A/cm}^2$ and $I_{02} = 1.6487 \text{ A/cm}^2$. These straight lines are known as the Tafel lines. The Tafel equation holds true only for $I_{fc} > 4I_0$ [6]. The other two solid lines are drawn based on (27) for the same I_0 values used previously. The Butler–Volmer equation is explicitly expressed in (27) if α_1 and α_2 are equal. For high cell

current densities, both equations have the same results. However, the error of the Tafel equation becomes large if $I_{fc} < 4I_0$, and the activation voltage calculated using (26) is negative for $I_{fc} < I_0$, as shown in Fig. 5. Therefore, the activation loss for all current densities is calculated using the inverse hyperbolic sine of (27)

$$V_{act} = \frac{RT}{F} \ln \left(\frac{I_{fc}}{I_0} \right) \quad (26)$$

$$V_{act} = \frac{RT}{F} \sinh^{-1} \left(\frac{I_{fc}}{2I_0} \right). \quad (27)$$

Alternatively, (27) can be written as (28), since it is easy to implement the equation in PSpice or Matlab/Simulink

$$V_{act} = \frac{RT}{F} \left(z + \sqrt{1 + z^2} \right) \quad (28)$$

where $z = (I_{fc}/2I_0)$.

It is evident from the graph that the exchange current I_0 of the two Tafel lines is not the same. This difference may occur for a number of reasons such as the cell temperature, reactant and product concentration, electrode material, its geometry, and so on [3], [6], [8], [10], [16]. The exchange current density can be expressed as [6], [23]

$$I_0 = A e^{-E_{act}/RT} \quad (29)$$

where $A = 101.2 \text{ kA/cm}^2$ is a preexponential factor obtained by curve fitting with the distributed model and $E_{act} = 120 \text{ kJ/mol}$ is the activation energy of the electrochemical reaction.

3) *Concentration Voltage Loss*: According to the polarization curve, this voltage drop appears when the current density of the fuel cell approaches the maximum current density of the cell and is dependent on the flow rate [10], [19]. The concentration loss is determined using (7). The cell current I_{fc} produced is related to the concentration of the species using the following:

$$I_{fc} = K \cdot (C_\infty - C_b). \quad (30)$$

The limiting current I_L is the cell current evaluated at $C_b = 0$. That is

$$I_L = K \cdot C_\infty. \quad (31)$$

Hence, the ratio of the concentration in (7) can be written alternatively as the ratio of the cell current to the limiting current of the fuel cell

$$\frac{C_b}{C_\infty} = 1 - \frac{I_{fc}}{I_L}. \quad (32)$$

Therefore, substituting (32) into (7), the concentration loss is written as

$$V_{con} = \frac{RT}{nF} \ln \left(1 - \frac{I_{fc}}{I_L} \right). \quad (33)$$

It is necessary to have experimental data for determination of the limiting current density. The limiting current density depends upon a number of things like reactant concentration, temperature, material properties, etc. Equation (31) can be alternatively expressed as [24]

$$I_L = K_L \frac{\ln(1 - p_{re})}{T} \quad (34)$$

where p_{re} is the reactant concentration, T is the operating temperature of the cell, and $K_L = 69$ is a constant factor.

C. Implementation of the SOFC Model Using PSpice

All the equations and the equivalent circuit of the lumped SOFC model discussed in the previous section are implemented in PSpice. The implemented model of the SOFC in PSpice is shown in Fig. 6. The PSpice model contains a circuit that represents the output voltage, as shown in Fig. 6(a), and equations that calculate the polarization losses and equivalent circuit of the flow rate conservation. Fig. 6(b) and (c) shows the activation and concentration losses, respectively, while the flow rate equivalent electrical circuit is shown in Fig. 6(d), where $n = 2$ for the hydrogen and water circuits and $n = 1$ for the oxygen circuit. The dynamics of the SOFC is embedded in the equivalent RC circuit. Moreover, the SOFC model is implemented in Matlab/Simulink for the development of emulator and control application. The parameters used in the simulation are given in Table II, where C_{H_2} , C_{H_2O} , and C_{O_2} are the capacitances of hydrogen, water, and oxygen, respectively.

IV. SIMULATION AND EXPERIMENTAL RESULTS

A. Experimental Test Setup

The experiments were carried out on an anode-supported tubular SOFC manufactured by NanoDynamics, Inc., Buffalo, NY. The anode material is nickel-yttria-stabilized zirconia, and the cathode is lanthanum strontium manganite. Pure hydrogen was supplied to the anode gas flow channel from a bank of cylinders through a flow controller. Compressed air regulated by a flow controller was provided through an electrical furnace to the cathode channel. The entire cell was kept well insulated to minimize the radiation heat loss from the system. The cell was heated up slowly by the hot air. When the cell temperature reached about $200 \text{ }^\circ\text{C}$, hydrogen was introduced, and the temperature was brought to $700 \text{ }^\circ\text{C}$. Once a steady open-circuit potential was obtained, the data collection was started. DC polarization of the cell was maintained by an electronic load controller run in constant-voltage mode. The $V-I$ data were collected while decreasing the voltage gradually to 0.5 V . While keeping the temperature constant, the data were collected at hydrogen flow rates of 31, 36, 41, and 51 mL/min. Then, the temperature was increased to $750 \text{ }^\circ\text{C}$, and the $V-I$ data were collected at all flow rates mentioned earlier. The same procedure was repeated at $800 \text{ }^\circ\text{C}$ and $850 \text{ }^\circ\text{C}$. At every flow and temperature, the data were collected after a steady-state condition was reached.

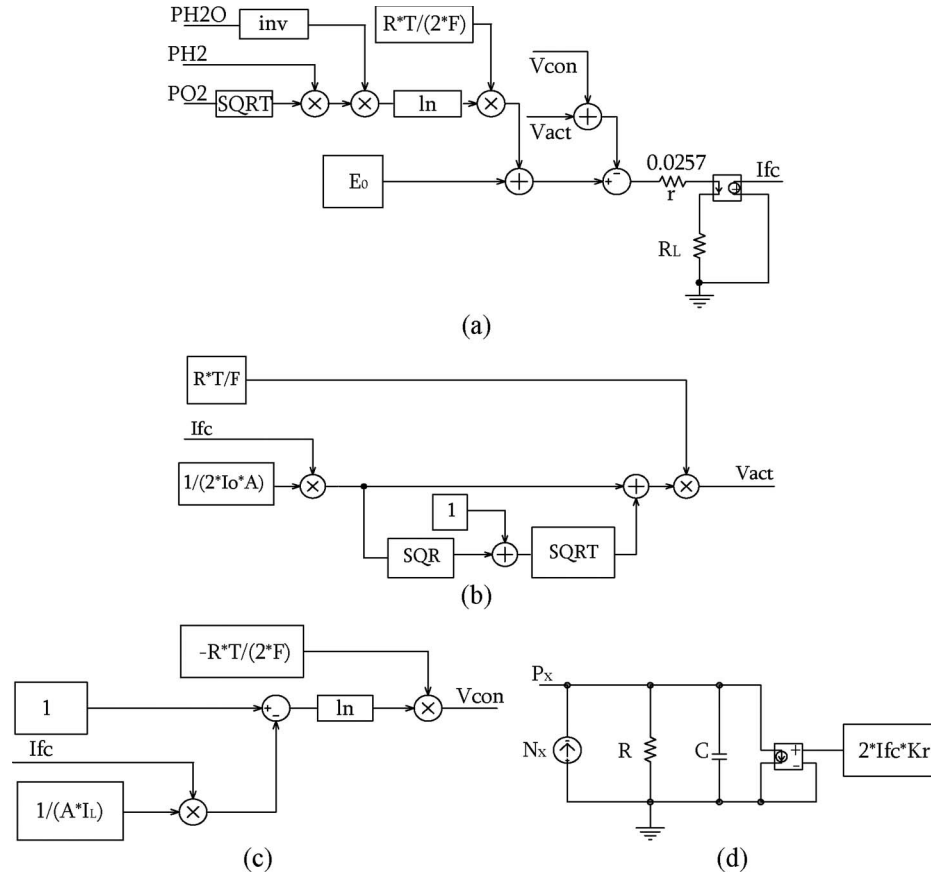


Fig. 6. PSpice simulation circuit diagram of an SOFC. (a) SOFC circuit diagram. (b) Activation loss. (c) Concentration loss. (d) Partial pressure circuit.

TABLE II
MODEL PARAMETERS

Parameter	Value	Unit
R_{H_2}	1.1826	$k\Omega$
R_{H_2O}	35.587	$k\Omega$
R_{O_2}	0.396	$k\Omega$
r	0.0257	Ω
Area	6.1412	cm^2
C_{H_2}	233.23	μF
C_{H_2O}	233.23	μF
C_{O_2}	734.84	μF

B. Steady-State Response of the SOFC Model

A single SOFC was simulated using PSpice based on the lumped model approach. The fuel cell was subjected to various flow rates and operating temperatures. As a result, the fuel cell exhibits different $V-I$ characteristics. Each $V-I$ point in the curve is generated by solving the dynamic model until the simulation reaches the steady state. The discussion on the simulation results is separated into the different $V-I$ curves based on the operating temperature and flow rate variations. The effects of the operating temperature and flow rate on the output voltage of the fuel cell is shown in Figs. 7–10. The output voltage of the cell depends on the operating temperature of the fuel cell and the natural logarithm of the reactant and product concentrations. The exchange current density changes with a change in the cell temperature, and the limiting current density varies, depending on the concentration of reactants and

products, which is reflected in the activation and concentration overpotentials. As a result, different $V-I$ curves are obtained for various operating cell temperatures and flow rates. If the fuel cell temperature is decreased at a given flow rate, the cell voltage decreases and vice versa. A reduction in flow rate for the same flow temperature will decrease the cell voltage and vice versa.

Comparisons between the experimental data and simulation results of the model for various flow rates and operating cell temperatures are shown in Figs. 7 and 8. Fig. 7 shows the $V-I$ curves of the different flow rates at 8000-°C cell temperature. Simulations at 850 °C for the same flow rate are also done. Fig. 8 shows the $V-I$ curves of the same flow rate at an operating cell temperature of 850 °C. Since the operating cell temperature is increased to 850 °C, the exchange current density is also increased. Fig. 9 shows the simulation $V-I$ curves at 800 °C and 850 °C of the four flow rates in a single graph. From the polarization curves, it can be seen that the cell voltage is almost the same for low cell current. As the cell current increases, the cell voltage starts to decrease almost linearly. However, the lower flow rate (31 mL/min) has a higher voltage drop with increasing cell current than the voltage drop with higher flow rates, as shown in Figs. 9(a) and (b). The sharp drop of each curve at high cell current is due to the limiting current density that depends on the flow rates.

The relative error between the experimental data and simulation results of the lumped model is shown in Table III. One point (from the experimental data -0.891 V) in the $V-I$ curve

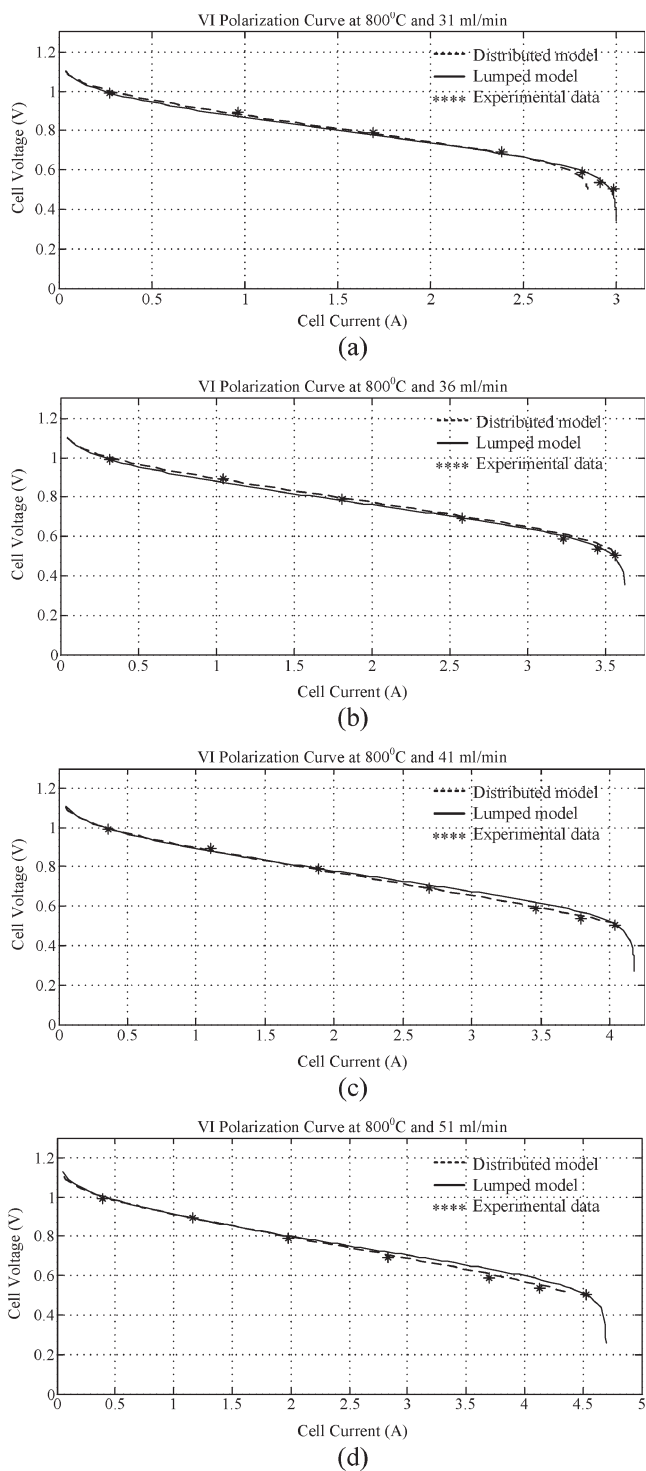


Fig. 7. $V-I$ curves for different input flow rates at 800 °C. (a) Polarization curves at 31 mL/min. (b) Polarization curves at 36 mL/min. (c) Polarization curves at 41 mL/min. (d) Polarization curves at 51 mL/min.

is set as a reference and then compared with the simulation results. The maximum relative error occurs at 31-mL/min flow rate and 800-°C cell temperature. The error becomes more severe for lower flow rate and cell temperature.

Simulation results at 41-mL/min flow rate were considered to study the effect of cell temperature on the cell voltage. Fig. 10(a) is a plot of the $V-I$ polarization curve at

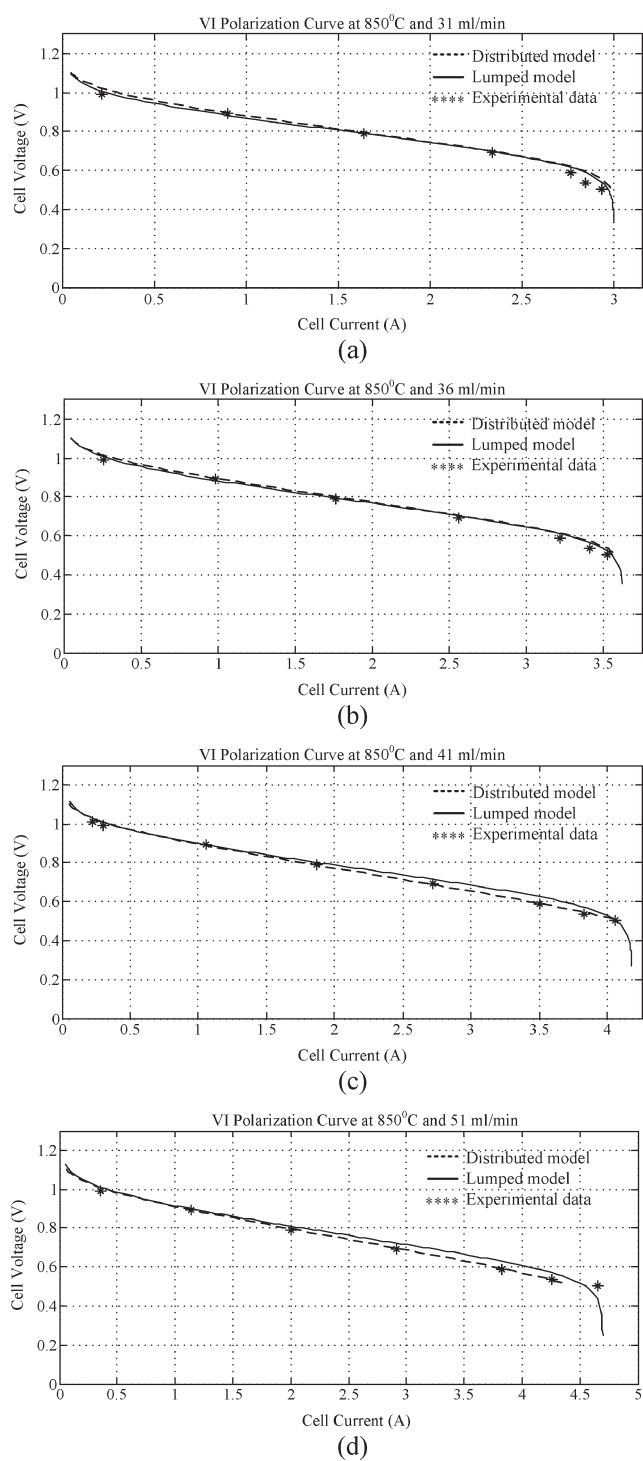


Fig. 8. $V-I$ curves for different input flow rates at 850 °C. (a) Polarization curves at 31 mL/min. (b) Polarization curves at 36 mL/min. (c) Polarization curves at 41 mL/min. (d) Polarization curves at 51 mL/min.

750-°C, 800-°C, and 850-°C cell temperatures. The cell voltage increases with an increase in the operating cell temperature. Fig. 10(b) is an enlarged portion of Fig. 10(a) at a cell current $I_{fc} = 2.5$ A. The cell voltage increases almost linearly as a function of temperature at this particular cell current and its vicinity, while the cell voltage is almost the same in the activation and concentration regions of the polarization curve.

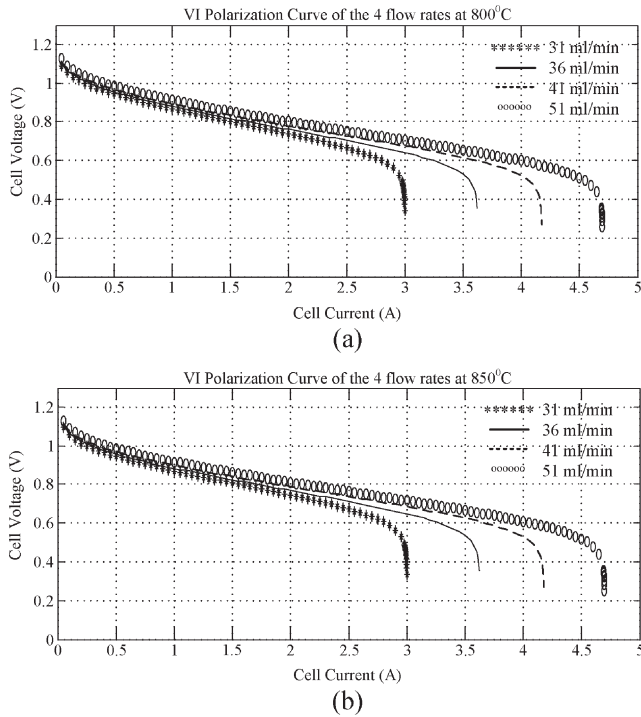


Fig. 9. Polarization curves at 800-°C and 850-°C operating temperatures and the four flow rates. (a) $V-I$ curves at 800-°C operating cell temperature. (b) $V-I$ curves at 850-°C operating cell temperature.

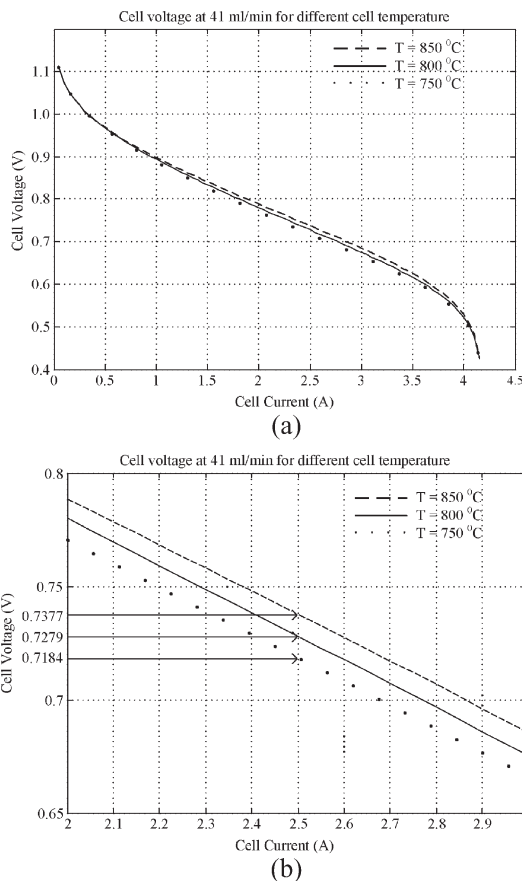


Fig. 10. Polarization curves at 41-mL/min flow rate and 750-°C, 800-°C, and 850-°C operating temperatures. (a) $V-I$ curves at 41 mL/min of the three operating cell temperatures. (b) Enlarged portion of $V-I$ curves given in (a) at cell current of 2.5 A.

TABLE III
RELATIVE ERRORS OF THE LUMPED SOFC MODEL

Temperature (°C)	Flow rate (ml/min)	Relative error
800	31	0.0192
	36	0.0175
	41	0.0099
	51	0.0006
850	31	0.0074
	36	0.0055
	41	0.0008
	51	0.0080

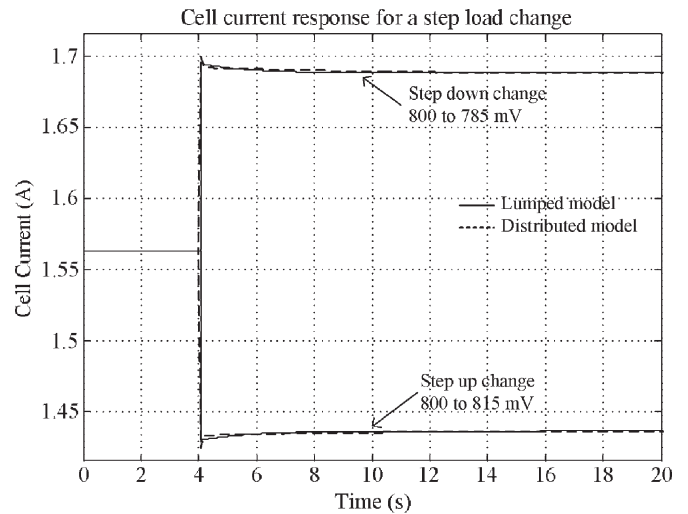


Fig. 11. Cell current response for a step load change.

C. Dynamic Response of the SOFC Model

The dynamic response of the model for a step change in the load at an operating cell temperature of 800 °C and a flow rate of 36 mL/min is considered. A step decrease of the cell voltage from 0.8 to 0.785 V was obtained at $t = 4.0$ s. The cell current increases from 1.563 to 1.695 A and slowly decays to its steady-state value of 1.688 A, as shown in Fig. 11. A step increase from 0.8 to 0.815 V in the cell voltage was also obtained at $t = 4.0$ s. The cell current drops from 1.563 to 1.429 A and then increases exponentially to 1.436 A, as shown in Fig. 11. The cell current response of the lumped model behaves in a manner similar to that of the distributed model with slight difference at time $t = 4.0$ s when the step change is applied. The cell current of the distributed model increases to 1.7 A during a step decrease in the cell voltage, which is higher than the cell current of 1.695 A of the lumped model. Similarly, the cell current of the distributed model drops to 1.425 A, which is lower than the cell current value of the lumped model when the cell voltage increases. Both models have similar time response. Fig. 12 shows the cell voltage transient for a step change in the cell current. The cell voltage jumps to 0.81 V and slowly reaches steady state for stepping down the cell current from 1.563 to 1.436 A. Similarly, when the cell current is stepped up from 1.563 to 1.695 A, the cell voltage drops to 0.79 V and finally settles to 0.785 V. The predicted cell voltage behaves in a manner similar to that of an actual fuel cell, as expected. It may be noted that the capacitance in the partial pressure circuit is a function of the cell temperature. However, it is observed

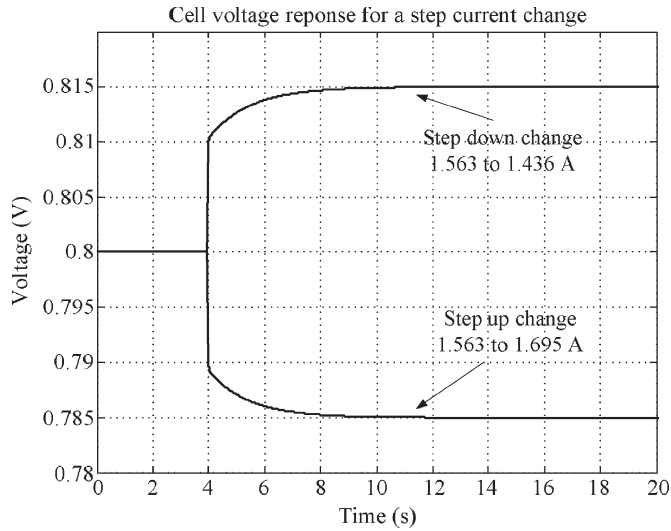


Fig. 12. Cell voltage response for a step change of the cell current.

that the response time does not change significantly with the cell temperature.

V. CONCLUSION

In this paper, a detailed steady-state model of a single SOFC was described. A lumped model was discussed that can be extended to model fuel cell stacks for real-time applications. The basic governing equations of the fuel cell were modeled with equivalent electrical circuits in order to simplify the system and achieve flexibility and easy tuning.

The steady-state simulation results of the lumped model agree with the experimental data and results of the distributed model. The capacitance in the simplified equivalent RC circuit can be changed to give the exact dynamic time response of the physical fuel cell. This SOFC model can be easily implemented in Matlab/Simulink and then programmed for real-time testing, which will help to study the performance of the fuel cell when subjected to external control.

APPENDIX A

BOUNDARY CONDITIONS FOR THE DISTRIBUTED MODEL

Number	Location	Boundary Condition (BC)	Remarks
BC1	$z = 0$	$C_i = C_{i,inlet}, i = H_2, H_2O$	Inlet Conditions
BC2	$r = R_{an}$	$-D_{H_2-H_2O_{eff}} A_{c,an} \frac{C_{H_2,an}}{dr} \Big _i = \frac{I_i}{2F}$ $D_{H_2-H_2O_{eff}} A_{c,an} \frac{C_{H_2O,an}}{dr} \Big _i = \frac{I_i}{2F}$	Flux Conditions
BC3	$z = \text{cathode channel length}$	$C_i = C_{i,inlet}, i = O_2, N_2$	Inlet Conditions
BC2	$r = R_{ca}$	$D_{O_2-N_2_{eff}} A_{c,ca} \frac{C_{O_2,ca}}{dr} \Big _i = \frac{I_i}{4F}$ $D_{N_2-O_2_{eff}} A_{c,ca} \frac{C_{N_2,ca}}{dr} \Big _i = 0$	Flux Conditions

R_{an} is outside the radius of the anode, R_{ca} is inside the radius of the cathode, and $A_{c,an}$ and $A_{c,ca}$ are the circumferential areas of the anode and cathode, respectively, at the electrolyte interface.

APPENDIX B

BOUNDARY CONDITIONS FOR THE LUMPED MODEL

Number	Location	Boundary Condition (BC)	Remarks
BC1	Anode	$N_x = N_{x,inlet}, x = H_2, H_2O$	Inlet Conditions
BC2	Cathode	$N_x = N_{x,inlet}, x = O_2$	Inlet Conditions

REFERENCES

- [1] D. J. Hall and R. G. Colclaser, "Transient modeling and simulation of a tubular solid oxide fuel cell," *IEEE Trans. Energy Convers.*, vol. 14, no. 3, pp. 749–753, Sep. 1999.
- [2] J. Padulles, G. W. Ault, and J. R. McDonald, "An integrated SOFC plant dynamic model for power system simulation," *J. Power Sources*, vol. 86, no. 1/2, pp. 495–500, Mar. 2000.
- [3] S. Nagata, A. Momma, T. Kato, and Y. Kasuga, "Numerical analysis of output characteristics of tubular SOFC with internal reformer," *J. Power Sources*, vol. 101, no. 1, pp. 60–71, Oct. 2001.
- [4] Y. Zhu and K. Tomsovic, "Development of models for analyzing the load-following performance of microturbines and fuel cells," *Elect. Power Syst. Res.*, vol. 62, no. 1, pp. 1–11, May 2002.
- [5] B. Kenney and K. Karan, "Mathematical micro-model of a solid oxide fuel cell composite cathode," in *Proc. Hydrogen Fuel Cells*, 2004.
- [6] A. Lazzaretto, A. Toffolo, and F. Zanon, "Parameter setting for a tubular SOFC simulation model," *J. Energy Resources Trans.*, vol. 126, no. 1, pp. 40–46, Mar. 2004.
- [7] D. A. Noren and M. A. Hoffman, "Clarifying the Butler–Volmer equation and related approximations for calculating activation losses in solid oxide fuel cell models," *J. Power Sources*, vol. 152, pp. 175–181, Dec. 2005.
- [8] F. Zhao and A. V. Virkar, "Dependence of polarization in anode-supported solid oxide fuel cells on various cell parameters," *J. Power Sources*, vol. 141, no. 1, pp. 79–95, Feb. 2005.
- [9] K. Sedghisigarchi and A. Feliachi, "Dynamic and transient analysis of power distribution systems with fuel cells—Part I: Fuel cell dynamic model," *IEEE Trans. Energy Convers.*, vol. 19, no. 2, pp. 423–428, Jun. 2004.
- [10] X. Xue, J. Tang, N. Sammes, and Y. Du, "Dynamic modeling of single tubular SOFC combining heat/mass transfer and electrochemical reaction effects," *J. Power Sources*, vol. 142, no. 1/2, pp. 211–222, Mar. 2005.
- [11] F. Jurado, "Novel fuzzy flux control for fuel-cell inverters," *IEEE Trans. Ind. Electron.*, vol. 52, no. 6, pp. 1707–1710, Dec. 2005.
- [12] Z. Jiang and R. A. Dougal, "A compact digitally controlled fuel cell/battery hybrid power source," *IEEE Trans. Ind. Electron.*, vol. 53, no. 4, pp. 1094–1104, Jun. 2006.
- [13] K. Jin and X. Ruan, "Hybrid full-bridge three-level LLC resonant converter—A novel DC–DC converter suitable for fuel-cell power system," *IEEE Trans. Ind. Electron.*, vol. 53, no. 5, pp. 1492–1503, Oct. 2006.
- [14] G. M. Martins, J. A. Pomilio, S. Buso, and G. Spiazzi, "Three-phase low-frequency commutation inverter for renewable energy systems," *IEEE Trans. Ind. Electron.*, vol. 53, no. 5, pp. 1522–1528, Oct. 2006.
- [15] M. Tekin, D. Hissel, M.-C. Pera, and J. M. Kauffmann, "Energy-management strategy for embedded fuel-cell systems using fuzzy logic," *IEEE Trans. Ind. Electron.*, vol. 54, no. 1, pp. 595–603, Feb. 2007.
- [16] R. Ramdamm, "Fuel cells—An introduction," in *Proc. Spec. Tech. Session Fuel Cells IEEE-PES Summer Meeting*, Vancouver, BC, Canada, Jul. 15–19, 2001, pp. 702–709.
- [17] Y. Qi, B. Huang, and K. T. Chuang, "Dynamic modeling of solid oxide fuel cell: The effect of diffusion and inherent impedance," *J. Power Sources*, vol. 150, pp. 32–47, Oct. 2005.
- [18] M. Iwata, T. Hikosaka, M. Morita, T. Iwanari, K. Ito, K. Onda, Y. Esaki, Y. Sakaki, and S. Nagata, "Performance analysis of planar-type unit SOFC considering current and temperature distributions," *Solid State Ionics*, vol. 132, no. 3, pp. 297–308, Jul. 2000.
- [19] J. E. Freech, J. W. Pratt, and J. Brouwer, "Development of a SOFC/gas turbine hybrid system model for aerospace applications," NASA, Washington, DC, NASA/TM-2004-213054, May 2004.
- [20] M. D. Lukas, K. Y. Lee, and H. Ghezal-Alagh, "Development of a stack simulation model for control study on direct reforming molten carbonate

fuel cell power plant," *IEEE Trans. Energy Convers.*, vol. 14, no. 4, pp. 1651–1657, Dec. 1999.

- [21] M. D. Lukas, K. Y. Lee, and H. Ghezal-Alagh, "An explicit dynamic model for direct reforming carbonate fuel cell stack," *IEEE Trans. Energy Convers.*, vol. 16, no. 3, pp. 289–295, Sep. 2001.
- [22] D. Bhattacharyya, R. Rengaswamy, and F. Caine, "Isothermal models for anode-supported tubular solid oxide fuel cells," *Chem. Eng. Sci.*, vol. 62, no. 16, pp. 4250–4267, Aug. 2007. DOI: 10.1016/j.ces.2007.04.020.
- [23] P. Famouri and R. Gemmen, "Electrochemical circuit model of a PEM fuel cell," in *Proc. IEEE Power Eng. Soc. Gen. Meeting*, Jul. 2003, vol. 3, pp. 1436–1440.
- [24] K. Huang, "Gas-diffusion process in a tubular cathode substrate of an SOFC," *J. Electrochem. Soc.*, vol. 151, no. 5, pp. A716–A719, 2004.



Abraham Gebregergis (S'07–M'08) received the B.S. degree from the University of Asmara, Asmara, Eritrea, in 2001, and the M.S. degree from Stellenbosch University, Stellenbosch, South Africa, in 2004. He is currently working toward the Ph.D. degree in electrical engineering in the Department of Electrical and Computer Engineering, Clarkson University, Potsdam, NY.

His research interests include power electronics, drives and machines, control, and fuel cell modeling.



Pragasen Pillay (S'84–M'87–SM'92–F'05) received the B.S. and M.S. degrees from the University of KwaZulu-Natal, Durban, South Africa, in 1981 and 1983, respectively, and the Ph.D. degree from the Virginia Polytechnic Institute and State University, Blacksburg, in 1987, while funded by a Fulbright Scholarship.

From January 1988 to August 1990, he was with the University of Newcastle upon Tyne, Newcastle upon Tyne, U.K. From August 1990 to August 1995, he was with the University of New Orleans,

New Orleans, LA. He is currently with Clarkson University, Potsdam, NY, where he is a Professor with the Department of Electrical and Computer Engineering and holds the Jean Newell Distinguished Professorship in Engineering. He has also been an Adjunct Professor with the University of Cape Town, Cape Town, South Africa, since 1999. He has organized and taught short courses on electric drives at the Annual Meeting of the IEEE Industry Applications Society. His research and teaching interests include modeling, design, and control of electric motors and drives for industrial and alternative energy applications.

Dr. Pillay is a Fellow of the Institution of Engineering and Technology, U.K., and a Chartered Electrical Engineer. He is a member of the Academy of Science of South Africa and the IEEE Power Engineering, IEEE Industry Applications, IEEE Industrial Electronics, and IEEE Power Electronics Societies. He is also a member of the IEEE Industry Applications Society (IAS) Electric Machines Committee, the Past Chairman of the IEEE IAS Industrial Drives Committee, and the Past Chairman of the IEEE Power Engineering Society Induction Machinery Subcommittee. He is currently the Chair of the Awards Committee of the IEEE IAS Industrial Power Conversion Department.



Debangsu Bhattacharyya received the B.S. degree from Regional Engineering College (currently National Institute of Technology), Durgapur, India, in 1993. He is currently working toward the Ph.D. degree in chemical engineering in the Department of Chemical Engineering, Clarkson University, Potsdam, NY.

He was with the refineries division of Indian Oil Corporation Ltd. in its Barauni Refinery. His research interests mainly include modeling, optimization, and control of fuel cells.



Raghunathan Rengaswamy received the B.S. degree from the Indian Institute of Technology (IIT), Madras, India, in 1990, and the Ph.D. degree from Purdue University, West Lafayette, IN, in 1995.

He is currently a Professor with the Department of Chemical Engineering, Clarkson University, Potsdam, NY. From 1996 to 2000, he was with IIT, Bombay, India. He was a Visiting Professor with the University of Delaware, Newark, in summer 1999; Purdue University, West Lafayette, IN, in winter 2001; and the University of Alberta, Edmonton, AB, Canada, in summer 2002. His research and teaching interests include modeling, optimization, diagnostics, and control of proton exchange membrane and solid oxide fuel cells, chemical process calculations, mathematical methods, computer-aided design, advanced process control, and artificial intelligence techniques in process engineering.

Dr. Rengaswamy was the recipient of the Young Engineer Award from the Indian National Academy of Engineering (INAE) in 2000. He was chosen by the students of the Department of Chemical Engineering, Clarkson University, as the Professor of the Year in 2003.